



Structural, optical and magnetic properties of $\text{Ni}_{1-x}\text{Zn}_x\text{O}/\text{Ni}$ nanocomposite

U. K. Panigrahi¹ · P. K. Das¹ · P. D. Babu² · N. C. Mishra³ · P. Mallick¹

© Springer Nature Switzerland AG 2019

Abstract

$\text{Ni}_{1-x}\text{Zn}_x\text{O}/\text{Ni}$ nanocomposite samples synthesized by wet chemical method were characterized by X-ray powder diffraction, Fourier Transform Infrared (FTIR) spectrometer, UV–Vis spectrometer and Nine Tesla Physical Property Measurement System (PPMS)-based vibrating sample magnetometer (VSM). XRD spectra contained peaks due to NiO and Ni. Rietveld refinement of XRD data indicated the change in lattice parameter is more than twice in NiO than in Ni suggests that Zn goes more favorably into NiO than in Ni. The band gap of NiO in $\text{Ni}_{1-x}\text{Zn}_x\text{O}/\text{Ni}$ samples increased from 3.58 to 3.81 eV with increasing x from 0 to 0.07 and thereafter the band gap slightly decreases. NiO/Ni nanocomposites show strong room temperature ferromagnetism. The ferromagnetic interaction further enhanced with 1% of Zn doping into NiO in NiO/Ni nanocomposite. Beyond this doping concentration, the magnetic interaction does not show any systematic variation. The observation of room temperature ferromagnetism in nanocomposite samples is explained by combining the effect of bound magnetic polaron and the magnetization of system with the distribution of magnetic ions as meagerly dispersed in large clusters. Our study indicated that $\text{Ni}_{0.99}\text{Zn}_{0.01}\text{O}/\text{Ni}$ nanocomposite sample could be useful for magnetic recording device application.

Keywords Nanocomposite · Doping · NiO · Ferromagnetism · Band gap

1 Introduction

Nanocomposites with at least one of the phase possessing nanoscale dimension [1] have attracted much attention of researchers due to their synergistic properties induced by the interactions between two or more different phases present in the system [2]. Despite challenges in the preparation of nanocluster phase with control of elemental composition and stoichiometry [3], nanocomposites unlock the possibility of developing advanced multifunctional devices due to the fascinating properties such as magnetic, magneto-optical, and semiconducting properties. Those properties can be modulated by the interfacial

interactions between the different nanocomponents present in the host composite [2, 4]. Among different nanocomposites, transition metal (TM)-based nanocomposites have been considered as model system due to their potential applications as catalysts [5], fuel-cell electrodes [6, 7], magnetic memories [8], supercapacitors/battery hybrids [9], etc. Among the TM-based nanocomposite, NiO/Ni system shows its potentiality for diverse application possibilities such as good absorption of dyes [10], energy efficient storage [11, 12], electrochemical storage [13], electrochemical performance [12], photocatalyst [13, 14], microwave absorber with high efficiency [15], magnetic

Electronic supplementary material The online version of this article (<https://doi.org/10.1007/s42452-019-0461-0>) contains supplementary material, which is available to authorized users.

✉ P. Mallick, pravanjanphy@gmail.com | ¹Department of Physics, North Orissa University, Baripada 757003, India. ²UGC-DAE Consortium for Scientific Research, Mumbai Centre, R-5 Shed, BARC, Mumbai 400085, India. ³Department of Physics, Utkal University, Bhubaneswar 751004, India.

SN Applied Sciences (2019) 1:438 | <https://doi.org/10.1007/s42452-019-0461-0>

Received: 16 January 2019 / Accepted: 4 April 2019 / Published online: 9 April 2019

recording device [16] and also the system imparts magnetic separation property [17].

Nickel oxide (NiO) with cubic structure is a type-II anti-ferromagnetic (AF) semiconductor showing direct wide band gap energy in the range from 3.6 to 4.3 eV [18–20]. Among the TM oxides, NiO reveals the highest Neel temperature (524 K) in its bulk phase [18, 21]. The replacement of Ni²⁺ by non-magnetic element like Zn would break the original AF order in the NiO matrix. One could expect the emergence of different magnetic properties at the expense of original AF order as well as the evolution of T_N due to doping. Master et al. [22] synthesized Zn-doped NiO by pulsed laser deposition method and demonstrated that NiO exhibits antiferro to ferromagnetic type behaviour due to the effect of Zn doping in field inducing spin canting of antiferromagnetic sublattices of NiO. Kumar et al. [23] also reported that NiO shows paramagnetism and superparamagnetism at 0.025 and 0.05 M Zn doping concentration, respectively. NiO shows room temperature ferromagnetism with further increasing Zn concentration (0.075 and 0.1 M). In another study, Bharati and Raji [24] reported that 2% Zn-doped NiO shows room temperature ferromagnetism. Huang et al. [25] reported that NiO/Ni nanocomposite exhibits much better electrochemical properties than pure NiO. Lai et al. [26] reported that NiO/Ni nanocomposite could be used for high-rate electrochemical energy storage device. Silva et al. [27] reported the improved room temperature saturation magnetization of NiO/Ni composite synthesized by proteic sol-gel method. You and Che [15] reported that the NiO/Ni nanoplate could be used as a highly efficient microwave absorber. Cui et al. [28] studied the effect of Mg dilution on the exchange bias properties of NiO/Ni granular system and reported that both exchange bias field and coercive field of the system decreased with Mg dilution. However, no literature is available on doping-induced evolution of properties of NiO/Ni nanocomposite.

In the present work, we synthesized Ni_{1-x}Zn_xO/Ni nanocomposite with an objective to enhance the magnetic properties of NiO/Ni composite by Zn doping. Our study indicated that the 1% Zn-doped NiO/Ni composite could be useful for magnetic recording device application.

2 Experimental

Ni_{1-x}Zn_xO/Ni nanocomposites with different Zn concentrations ($x=0, 0.01, 0.03, 0.05, 0.07, 0.1$) were prepared by wet chemical method using Ni(NO₃)₂·6H₂O and Zn(CH₃COO)₂·2H₂O as initial precursor. The stoichiometric amount of the precursor materials along with 2 g of polyvinyl pyrrolidone (PVP) was dissolved in distilled water to form a solution. The solution was homogenized by stirring

for 1 h with the help of magnetic stirrer. The resultant solutions were dried in a hot plate and finally, the dried products were sintered at 300 °C for 1 h to obtain Ni_{1-x}Zn_xO/Ni nanocomposite samples. It is worth mentioning here that the pure NiO sample was synthesized without taking PVP.

Structural and microstructural characterization of NiO and Ni_{1-x}Zn_xO/Ni samples were done using Bruker X-ray diffractometer (Model: D8 Advance) operating with CuK α radiation ($\lambda = 1.540598 \text{ \AA}$). The optical band gap of the samples was determined using diffuse reflectance spectroscopy by a double-beam UV-Vis spectrometer (Shimadzu, UV-2450) operated with integrating sphere assembly. The functional group analyses of the samples were done by the characterization with FTIR (Shimadzu, IRAffinity-1) spectrophotometer. A quantum design Nine Tesla (9T) Physical Properties Measurement System (PPMS)-based vibrating sample magnetometer (Model No: 6700) was employed to measure magnetic properties of the samples.

3 Results and discussion

3.1 Structural properties

Figure 1 shows the XRD pattern of Ni_{1-x}Zn_xO/Ni nanocomposites with different Zn concentrations. As shown in the figure, the nanocomposite samples contain Ni (JCPDS card no: 65-2865) and NiO (JCPDS card no: 73-0179) phase without any other impurity phase. The XRD pattern of pure NiO and the standard XRD pattern for ZnO (JCPDS card

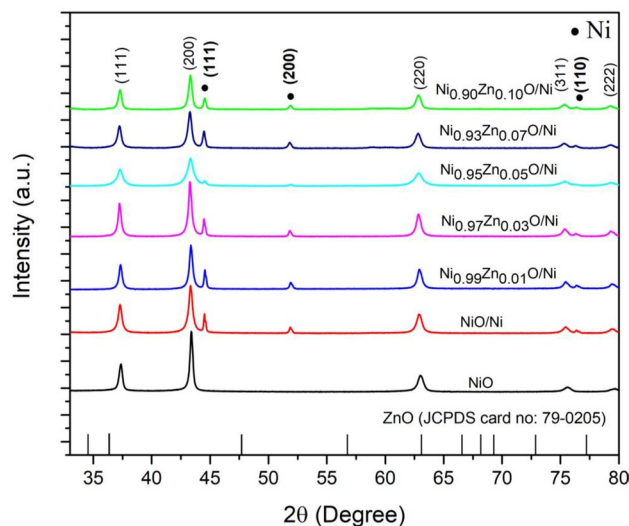


Fig. 1 XRD pattern of NiO and Ni_{1-x}Zn_xO/Ni composite samples with different Zn concentrations ($x=0, 0.01, 0.03, 0.05, 0.07, 0.1$). The standard XRD pattern for ZnO (JCPDS card no: 79-0205) is given for comparison

no: 79-0205) are also given in Fig. 1 for comparison. Zn doping in NiO/Ni composite does not affect the crystal structure of either NiO or Ni. Nor did it induce any impurity phase in the sample. However, the microstructural parameters like lattice parameter, bond length, etc. [29] of composite sample is affected by Zn doping. It is clear from Rietveld refinement of XRD data using FullProf [30] that the variation of lattice parameters of NiO and Ni is not remarkable but slowly increases with increasing Zn concentration (Table 1). The percentage of change of lattice parameter in NiO is more than twice than in Ni in the composite sample with the highest Zn doping concentration, i.e., 10%. This suggests that Zn goes more favorably into NiO than in Ni. Figure 2 shows the representative Rietveld refinement image of $\text{Ni}_{0.9}\text{Zn}_{0.1}\text{O}/\text{Ni}$ nanocomposite. The increase in lattice parameter could be due to the substitution of Ni atoms with the smaller Shannon ionic radii (0.69 Å) by Zn atoms of larger Shannon ionic radii (0.74 Å) in the $\text{Ni}_{1-x}\text{Zn}_x\text{O}/\text{Ni}$ composite [31]. We also extracted the Ni–Ni, Ni–O and O–O bond length from the Rietveld refinement and presented those in Table 1. The Ni–O bond length in NiO of 2.0862 Å is consistent with the reported values [32]. The substitution of Zn in place of Ni in NiO lattice could affect the values of near neighbor and next near neighbor bond lengths of the composite samples [32], as a result of which the bond lengths (Table 1) increased with increasing Zn doping concentration.

3.2 Functional group analysis

FTIR spectroscopy is used to study the presence of functional groups in the samples. The representative FTIR spectra of pure NiO, NiO/Ni and 1% Zn-doped NiO/Ni is shown in Fig. 3. The broad absorption band observed at $\sim 3630\text{ cm}^{-1}$ in NiO/Ni sample is attributed to the OH stretching vibrations of water molecules present in the

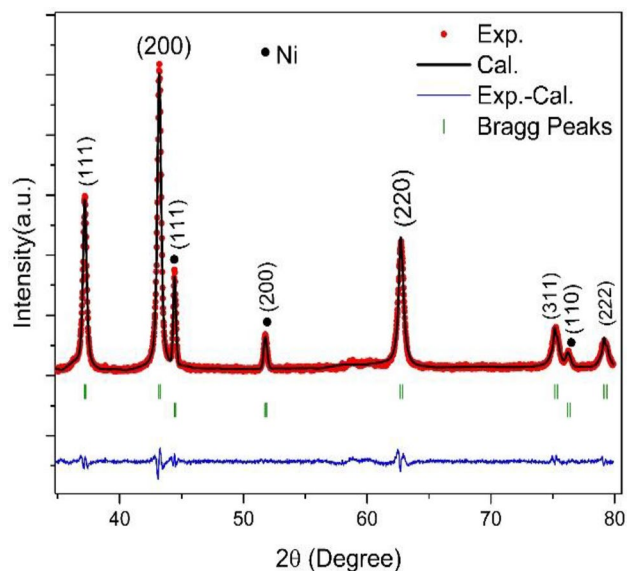


Fig. 2 Rietveld Refinement of the typical XRD pattern of $\text{Ni}_{0.9}\text{Zn}_{0.1}\text{O}/\text{Ni}$ nanocomposite

samples [33, 34]. This band is shifted to lower wavenumber with increasing Zn concentration in NiO. It has been predicted theoretically that the frequency lowering of the stretch motions of water could be due to the combined effect of an harmonicity of the considered potential and environment [35–39]. The redshift of OH stretching vibrations with increasing Zn concentration in NiO could be due to effect of Zn doping-induced modification in chemical environment. The appearance of broad absorption band at $\sim 447\text{ cm}^{-1}$ in all samples in our case could also be assigned to the stretching modes Ni–O [23, 40]. The observations of other different bands in NiO and Zn-doped NiO/Ni samples are summarized in Table 2 along with corresponding reported values.

Table 1 Bond length, lattice parameter and % of NiO phase in NiO and $\text{Ni}_{1-x}\text{Zn}_x\text{O}/\text{Ni}$ nanocomposite samples. The R_p , R_{wp} and goodness of fit (χ^2) values for each sample are given for comparison

Sample	Bond length (Å)			Lattice parameter (Å)		Change in lattice parameter (%)		% of NiO phase	R_p	R_{wp}	χ^2
	Ni–Ni	Ni–O	O–O	NiO	Ni	NiO	Ni				
NiO	2.9504	2.0862	2.9504	4.1725	–	0	–	100	13.2	8.14	2.66
NiO/Ni	2.9559	2.0902	2.9559	4.1803	3.5259	0.19	0	91.15	13.4	8.63	3.18
$\text{Ni}_{0.99}\text{Zn}_{0.01}\text{O}/\text{Ni}$	2.9572	2.0910	2.9572	4.1820	3.5276	0.23	0.05	89.18	14.5	8.96	2.90
$\text{Ni}_{0.97}\text{Zn}_{0.03}\text{O}/\text{Ni}$	2.9577	2.0914	2.9577	4.1828	3.5279	0.25	0.06	90.07	13.4	9.04	3.73
$\text{Ni}_{0.95}\text{Zn}_{0.05}\text{O}/\text{Ni}$	2.9610	2.0937	2.9610	4.1875	3.5293	0.36	0.1	96.40	12.7	8.86	2.50
$\text{Ni}_{0.93}\text{Zn}_{0.07}\text{O}/\text{Ni}$	2.9605	2.0934	2.9605	4.1868	3.5309	0.34	0.14	87.28	16.5	10.1	3.25
$\text{Ni}_{0.9}\text{Zn}_{0.1}\text{O}/\text{Ni}$	2.9619	2.0944	2.9619	4.1888	3.5312	0.39	0.15	87.31	19.6	11.6	3.72

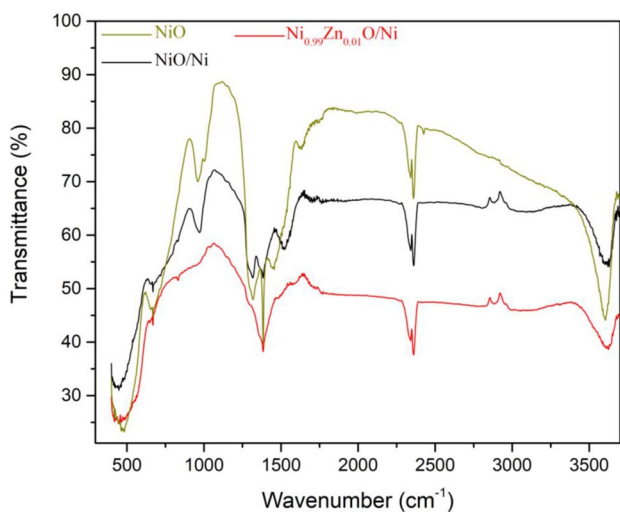


Fig. 3 Representative FTIR spectra of NiO, NiO/Ni and 1% Zn-doped NiO/Ni composite samples

3.3 Optical properties

The optical absorption coefficient (α) and optical band gap (E_g) are related by following relation [51]:

$$\alpha = B \frac{(h\nu - E_g)^p}{h\nu} \tag{1}$$

where $h\nu$ is the photon energy and B is a material dependent constant parameter. The value of p is taken to be 1/2 for direct transition and 2 for indirect transition. Since NiO is a direct band gap semiconductor [52], we therefore consider p as 1/2. From the Tauc plot ($(\alpha h\nu)^2 \sim h\nu$), we calculate the band gap of NiO and Zn-doped NiO/Ni samples

by extrapolating the linear portion of the curve to zero photon energy. The value of E_g as obtained for pure NiO is 3.83 eV (Fig. 4) which is consistent with the literature [53].

Singh et al. [31] synthesized $Ni_{1-x}Zn_xO$ solid solution by solid-state reaction and reported that band gap of NiO decrease in 3.65 to 3.35 eV with increasing Zn concentration from 0 to 31% in NiO. Thangamani and Pushpanathan [50] also reported the decrease in band from 3.70 to 3.58 eV with increasing Zn concentration from 0 to 5% in NiO prepared by chemical precipitation method. Similar observation, i.e., decrease in band gap with increasing Zn concentration, has also been reported for Zn-doped NiO thin film cases [41, 54–56]. In contrary to the literature, our study indicated that the band gap of NiO increased from 3.58 to 3.81 eV with increasing of Zn concentration 0 to 7% in $Ni_{1-x}Zn_xO/Ni$ nanocomposites and thereafter the band gap slightly decreases for 10% Zn-doped NiO/Ni sample (Fig. 5). Since the band gap of ZnO showing rock salt structure is ~ 4.5 eV [57], therefore one should expect that the band gap of NiO with rock salt structure will be increased with Zn doping.

Generally, the band gap of ternary compound shows bowing. We extracted the bowing parameter for $Ni_{1-x}Zn_xO/Ni$ nanocomposites by fitting the band gap data to the following relation [58, 59]:

$$E_{g,Ni_{1-x}Zn_xO} = xE_{g,ZnO} + (1-x)E_{g,NiO} - bx(1-x) \tag{2}$$

where $E_{g,Ni_{1-x}Zn_xO}$, $E_{g,ZnO}$ and $E_{g,NiO}$ are the band gap of $Ni_{1-x}Zn_xO/Ni$ nanocomposite, ZnO and NiO, respectively. The nonlinearity in the band gap is determined by the bowing parameter (b). Since the Zn is doped in the rock salt structure of NiO, we therefore considered the band gap of rock salt ZnO and experimentally obtained band gap of $Ni_{1-x}Zn_xO/Ni$ nanocomposite with Zn concentration

Table 2 Vibrational bands observed for NiO and $Ni_{1-x}Zn_xO/Ni$ with different values of x

Assigned vibrational band	Band (cm^{-1}) observed for different samples							Reported value of band
	NiO	$Ni_{1-x}Zn_xO/Ni$ with different values of x						
		0	0.01	0.03	0.05	0.07	0.10	
Ni–O stretching mode	$\sim 447; 484$	~ 447	~ 447	~ 447	~ 447	~ 447	~ 447	443 to 432 [23]; 436 [41]; 480 [42]
Stretching and bending vibrations of the intercalated C–O species	669	669	669	669	669	669	669	670 [42]
C–H vibrational bond	719	719	719	719	719	719	719	719 [43]
Bending vibrations of CO_3^{2-} ion	–	–	833	831	831	–	–	831 [44]
trans-C–H out-of-plane bend	960	972	–	–	–	974	974	960–970 [45]
C–O stretching vibration	–	–	1045	1043	1045	–	–	1045 [46]
Bending vibrations of CO_3^{2-} ion	1384	1385	1385	1385	1385	1385	1385	1384 [44]
Absorption of CO_2 molecule from air	2358	2360	2360	2358	2360	2358	2358	2357 [47]
Stretching vibration of C–H bond	–	2802	2829	2818	2827	2804	2808	2830 [42]; 2805 [48]
–	–	2885.5	2885.5	2885.5	2885.5	2885.5	2885.5	2882 [49]
O–H stretching vibrations	3604	3630	3626	3620	3603	3604	3604	3641 [50]

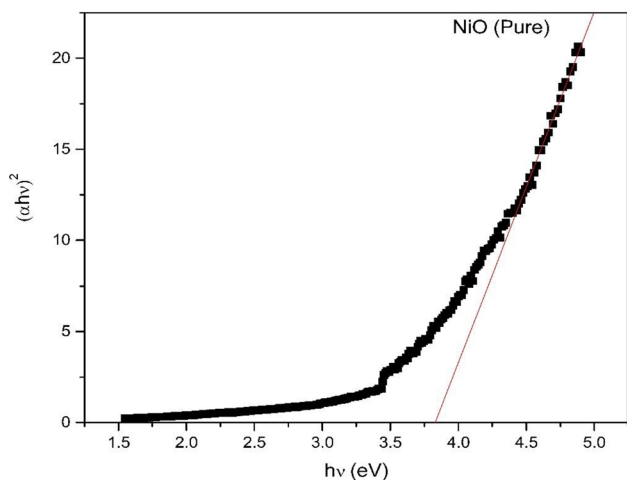


Fig. 4 Variation of $(\alpha hv)^2$ versus $h\nu$ for NiO nanoparticles

to fit the same into Eq. (2). Considering the reported experimental and theoretical values of $E_{g,ZnO}$ of rock salt ZnO as 4.5 eV and 4.27 eV [57], respectively, we obtain the value of b as -1.81 eV and -2.06 eV, respectively. Singh et al. [31] reported the value of bowing parameter as -0.93 eV and pointed out that the negative bowing could possibly due to the repulsive interaction between the O-2p ligand and Ni-3d orbital.

Refractive index (n) is one of the important properties to evaluate the potentiality of the material in the application of

integrated optical devices. Kumar and Singh [60] have proposed a model to calculate n for mixed materials belonging to semiconductors of different groups, insulators and halides. According to the model, the E_g and n are related by

$$n = KE_g^C \tag{3}$$

where $K=3.3668$ and $C=-0.32234$. We calculate n for each of the composite sample from the E_g of corresponding NiO using Eq. (3). We also calculate the $\alpha'_{\text{Classical}}$ and α' from n and E_g respectively using the following relation [61–63]:

$$\alpha'_{\text{Classical}} = \frac{(n^2 - 1)}{(n^2 + 2)} \frac{M}{\rho} \times 0.395 \times 10^{-24} \text{cm}^3 \tag{4a}$$

$$\alpha' = \left[\frac{12.41 - 3\sqrt{E_g - 0.365}}{12.41} \right] \frac{M}{\rho} \times 0.395 \times 10^{-24} \text{cm}^3 \tag{4b}$$

where M and ρ are the molecular weight (g/mol) and density of required material (g/cm³). The calculated values of E_g , n , $\alpha'_{\text{Classical}}$ and α' of NiO present in Ni_{1-x}Zn_xO/Ni nanocomposite samples are given in Table 3. The values of refractive index and electronic polarizability of NiO decreased with increasing Zn concentration in NiO/Ni nanocomposite. The deviation from the trend of variation of E_g and other parameters with Zn content (Table 3) for

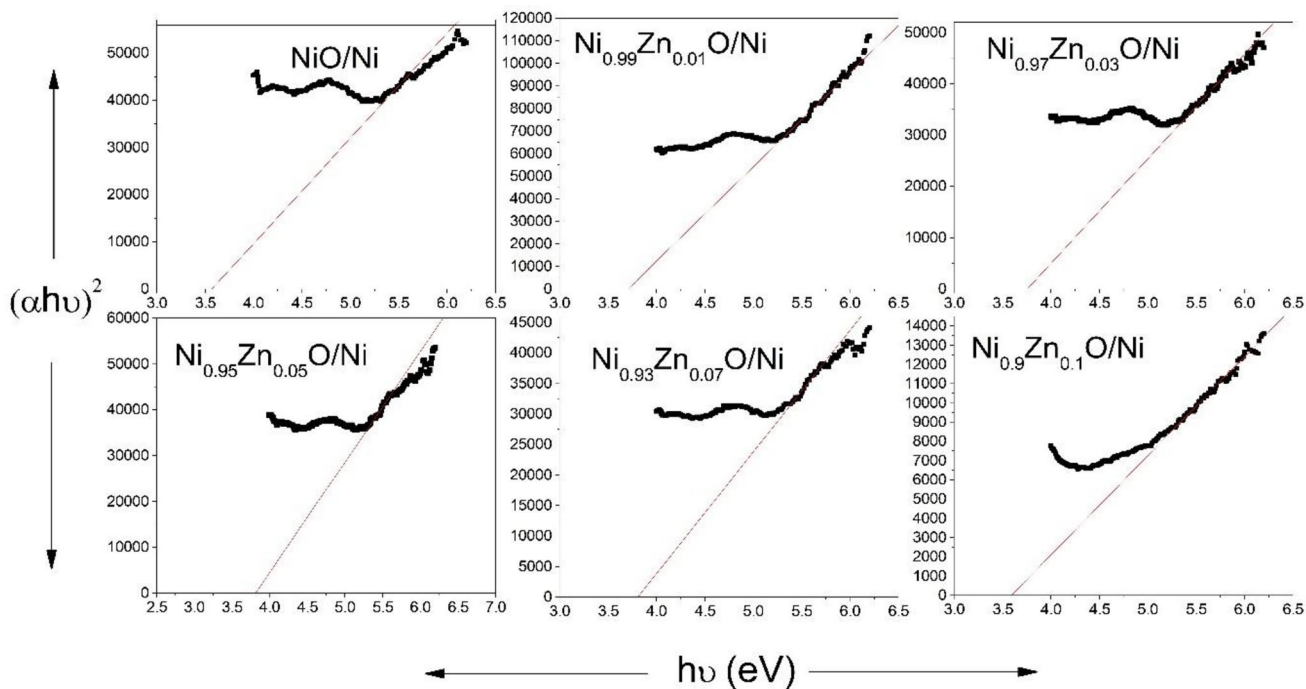


Fig. 5 Variation of $(\alpha hv)^2$ versus $h\nu$ for NiO/Ni and Zn-doped NiO/Ni nanocomposite samples

Table 3 The values of E_g , n , $\alpha'_{\text{Classical}}$ and α' of NiO in $\text{Ni}_{1-x}\text{Zn}_x\text{O}/\text{Ni}$ nanocomposite samples

Sample	E_g (eV)	n	$\alpha'_{\text{Classical}}$ ($\times 10^{-24}$ cm ³)	α' ($\times 10^{-24}$ cm ³)
NiO	3.8284	2.1841	2.4633	2.4333
NiO/Ni	3.5848	2.2309	2.5213	2.5046
$\text{Ni}_{0.99}\text{Zn}_{0.01}\text{O}/\text{Ni}$	3.7092	2.2065	2.4914	2.4678
$\text{Ni}_{0.97}\text{Zn}_{0.03}\text{O}/\text{Ni}$	3.7552	2.1978	2.4805	2.4544
$\text{Ni}_{0.95}\text{Zn}_{0.05}\text{O}/\text{Ni}$	3.7907	2.1911	2.4721	2.4442
$\text{Ni}_{0.93}\text{Zn}_{0.07}\text{O}/\text{Ni}$	3.8105	2.1874	2.4675	2.4384
$\text{Ni}_{0.9}\text{Zn}_{0.1}\text{O}/\text{Ni}$	3.6033	2.2272	2.5169	2.4991

the highest Zn content (10%) in the sample could possibly due to phase segregation and second phase precipitation in the sample.

3.4 Magnetic properties

Figure 6 shows the zero field cooled (ZFC) and field cooled (FC) magnetization of NiO nanoparticle in the temperature range 3 to 360 K measured at a field of 100 Oe. Initially, both ZFC and FC magnetization slowly increase with decreasing temperature from 360 K and the bifurcation in the ZFC and FC data starts at ~ 310 K. The ZFC data shows a broad peak at ~ 170 K and then decreased up to ~ 140 K. Again, the ZFC curve shows a monotonic increase with further lower the measuring temperature. The FC curve increases monotonically with decreasing temperature. The continuous increase in both FC and ZFC magnetization with lowering the temperature below 140 K indicated the signature of non-interacting or weak interacting particles [64–66]. Similar observation has been reported by Tadic et al. [66] for NiO nanoparticles embedded in a silica matrix.

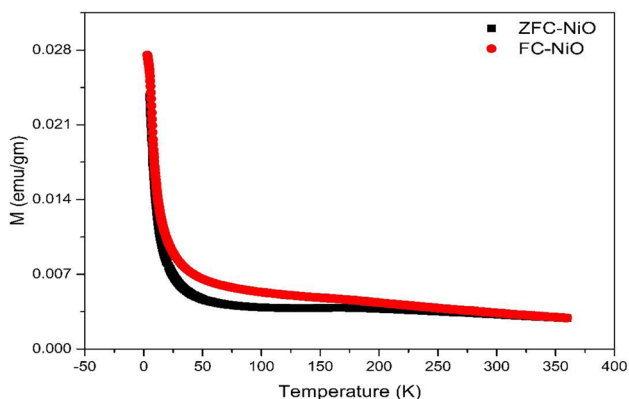


Fig. 6 Variation of ZFC and FC magnetization of NiO as a function of temperature measured at an applied field of 100 Oe

The appearance of broad peak at 170 K in NiO could be the occurrence of blocked and relaxed superparamagnetism due to the interaction of ferromagnetic surface spin and antiferromagnetic core. The interaction between surface and core of NiO nanoparticles could result into ferromagnetic like hysteresis loop with missing saturation behavior (discussed later) as the antiferromagnetic exchange interaction between the core spins cannot be completely released in measured magnetic field [67].

To probe further into the magnetic behavior of NiO, we plot inverse susceptibility (χ^{-1}) as a function of temperature (T) (Fig. 7). As indicated from the figure, NiO shows paramagnetic like behavior due to incomplete compensation of AFM sublattices at the surface [68]. In Langevin’s statistical theory of paramagnetism, the thermal variation of susceptibility is expressed as [69]:

$$\chi = \frac{N\mu_{\text{eff}}^2}{3kT} = \frac{C}{T} \tag{5}$$

where $C = \frac{N\mu_{\text{eff}}^2}{3k_B}$. The Curie constant (C) of 0.02018934 is obtained by the linear fit of the $\chi^{-1} \sim T$ at high-temperature regime. The effective moment (μ_{eff}) of NiO can be calculated from C using the relation [70]:

$$\mu_{\text{eff}} = 2.828\sqrt{C} \tag{6}$$

Effective magnetic moment of the NiO nanoparticles thus calculated is $3.47 \mu_B$, which is close to both theoretical ($2.83 \mu_B$) as well as experimental (2.8 to $4.0 \mu_B$) value for Ni^{2+} ion [71].

Figure 8 shows the ZFC and FC magnetization of $\text{Ni}_{1-x}\text{Zn}_x\text{O}/\text{Ni}$ nanocomposite samples at different Zn doping concentration. As shown in the figure, all the nanocomposite samples show a clear minima (T_m) in the ZFC curve up to which the magnetic moment decreases

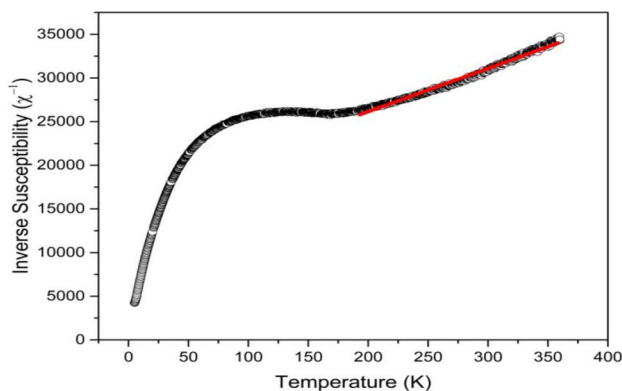


Fig. 7 Variation of inverse susceptibility with temperature of NiO samples and red line corresponds to linear fitting at high-temperature regime

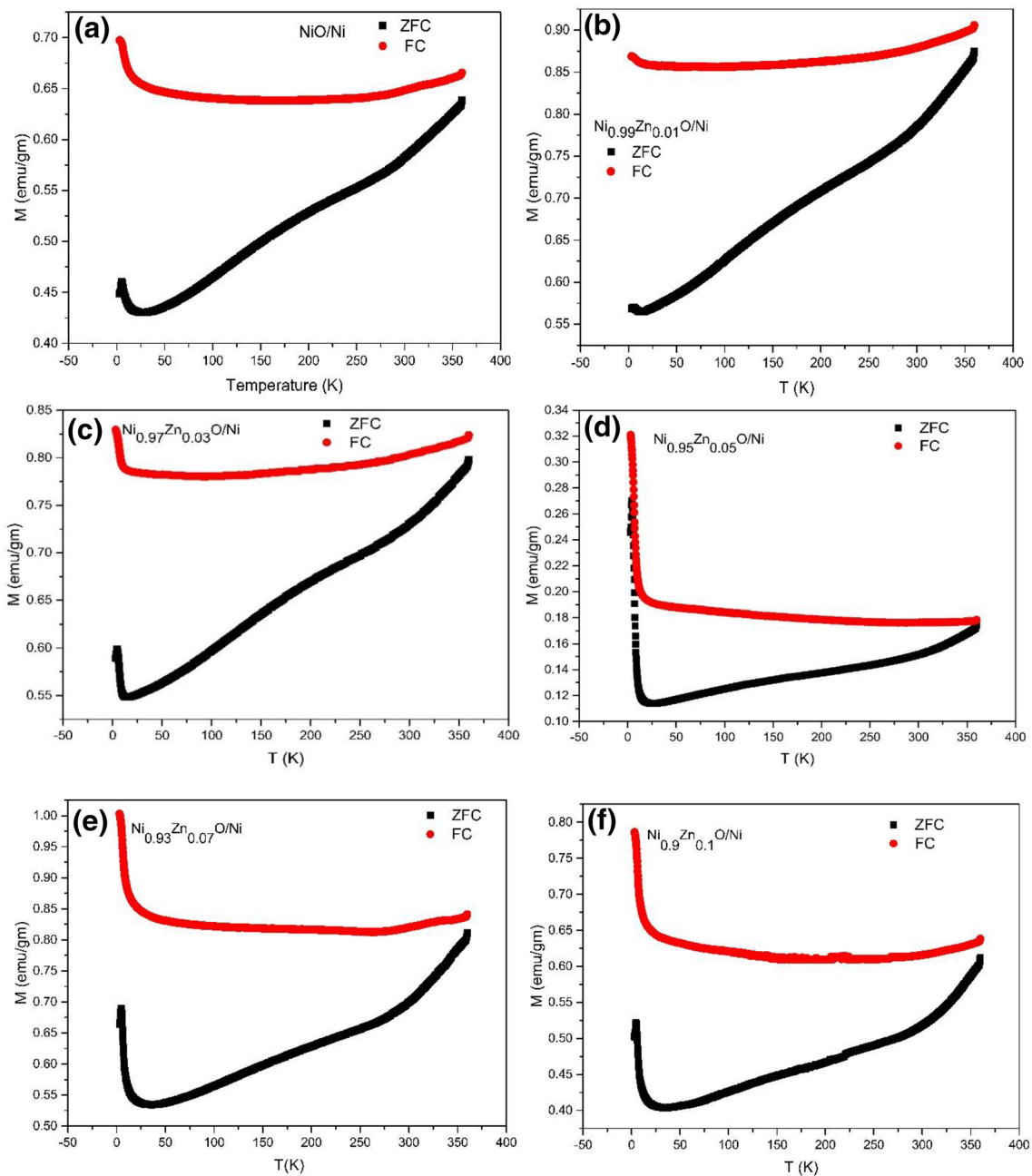


Fig. 8 ZFC and FC magnetization as a function of temperature measured at $H = 100$ Oe for **a** NiO/Ni, **b** $\text{Ni}_{0.99}\text{Zn}_{0.01}\text{O}/\text{Ni}$, **c** $\text{Ni}_{0.97}\text{Zn}_{0.03}\text{O}/\text{Ni}$, **d** $\text{Ni}_{0.95}\text{Zn}_{0.05}\text{O}/\text{Ni}$, **e** $\text{Ni}_{0.93}\text{Zn}_{0.07}\text{O}/\text{Ni}$ and **f** $\text{Ni}_{0.9}\text{Zn}_{0.1}\text{O}/\text{Ni}$

with an increase in temperature and thereafter the magnetic moment increases with temperature. The increase in ZFC magnetization below T_m could possibly be due to the paramagnetic contribution of loose surface spin of the particles [72]. The value of T_m does not show any systematic variation with Zn doping. The T_m value of $\text{Ni}_{1-x}\text{Zn}_x/\text{Ni}$ sample decreased from 25 K to 14 K with increasing x from 0 to 3% and the same further increased to 30 K with increasing x to 10%. The non-monotonic variation of T_m

with Zn content (x) may be due to second phase precipitation at high Zn content as discussed earlier. The merging of ZFC and FC magnetization and maxima in ZFC curve above T_m , which was seen in case of NiO sample (Fig. 6), could not be achieved in the NiO/Ni or the Zn-doped NiO/Ni samples in measured temperature range. This indicates that the occurrence of irreversibility temperature as well as blocking temperature in nanocomposite samples is higher than 360 K [16] and possibly due to the large average size of the

Ni particles and increased anisotropy due to the coupling in Ni/NiO (ferromagnetic/antiferromagnetic) system [8]. The behavior of ZFC curve reflects two magnetic phases viz. one paramagnetic which dominate in low-temperature region and the other ferromagnetic contribution which predominates in the higher temperature region [73, 74].

To further understand the magnetic behavior of NiO and Ni_{1-x}Zn_xO/Ni nanocomposite, magnetization as a function of field (M-H) was recorded at room temperature (Fig. 9). The inset of figure (Fig. 9) shows the expanded view of M-H curve for pure NiO showing hysteresis loop. As shown in figure, NiO nanoparticles exhibit ferromagnetic like hysteresis loop with missing saturation behavior. This could possibly due to interaction between antiferromagnetic core and ferromagnetic surface spin in the core-shell structure [67, 75]. In addition to weak ferromagnetism of NiO, Ni moments also contribute to net magnetization in NiO/Ni nanocomposite. Hence the appearance of strong ferromagnetism is reflected in the M-H curve of NiO/Ni nanocomposite. The

ferromagnetic interaction further enhanced with 1% of Zn doping into NiO in NiO/Ni nanocomposite. The random substitution of non-magnetic Zn at Ni sites of NiO leads to the formation of Ni-O-Zn-O-Ni which in turn breaks the original Ni-O-Ni-O-Ni antiferromagnetic superexchange interaction [28, 76, 77]. As a result of which ferromagnetic interaction amplified with 1% of Zn doping. The magnetic interaction starts decreasing with further increasing Zn concentration in NiO/Ni nanocomposite. The 5% Zn-doped NiO/Ni sample with the lowest percentage of Ni phase (~3.6%) shows the lowest value of magnetization (Table 4) among all nanocomposite samples. The intrinsic non-stoichiometry of ZnO, i.e., Zn excess nature also plays the crucial role in determining the magnetic property of NiO/Ni nanocomposite at higher doping concentrations. As the Zn doping percentage in NiO/Ni increases, the metal excess nature of ZnO dominates over metal deficient NiO which in turn reduces the percentage of Ni fraction in the composite sample. Since the fraction of Ni phase reduces, the magnetic interaction reduces. The magnetization increased further with increasing Zn doping concentration to 7% and the same again decreased at the highest Zn doping concentration (10%). The increase and decrease in magnetic interaction Zn concentration > 5% could possibly due to the competition between effect seen at low doping concentration and the dominance of intrinsic non-stoichiometry of ZnO.

There are several models proposed in the literature to understand the origin of ferromagnetism (FM) in doped oxide systems. The bound magnetic polaron (BMP) model is one of the models which is partially explain the origin of room temperature ferromagnetism in transition metal (TM)-doped oxide materials. The presence of magnetic cations, carriers, and defects like oxygen vacancies in the system can make up BMPs which may be responsible for the occurrence of room temperature FM in the oxide materials [78, 79]. According to BMP model [80–83], the magnetization is given by

$$M = M_0L(x) + \chi_m H \tag{7a}$$

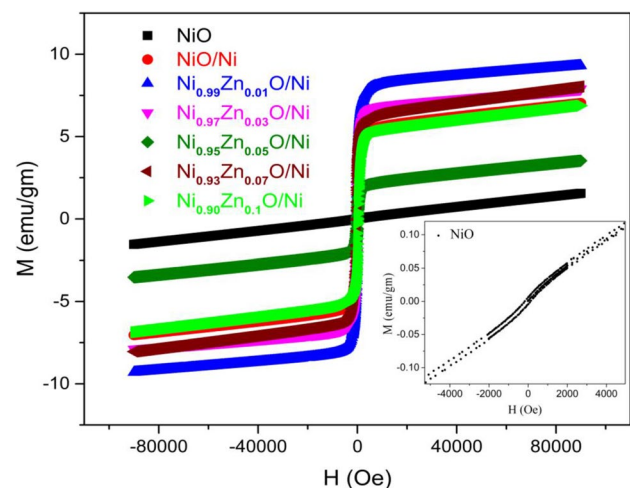


Fig. 9 M-H curve of NiO and Ni_{1-x}Zn_xO/Ni nanocomposite samples measured at 300 K. Inset shows the expanded view of M-H curve for NiO

Table 4 Various parameters extracted from M-H curves of NiO and Ni_{1-x}Zn_xO/Ni (x=0 to 10) nanocomposite samples. The % of Ni phase given in table was obtained from Rietveld refinement of XRD data

Sample	<i>M_r</i> (emu/g)	<i>H_c</i> (Oe)	% of Ni phase	<i>M₀</i> (emu/g)	<i>N</i> (× 10 ¹⁷ cm ⁻³)	<i>m_{eff}</i> (× 10 ⁻¹⁷ emu)	<i>χ_m</i>	<i>M_S</i> (emu/g)	<i>K₁</i> (× 10 ⁴) (erg/g)
NiO	0.005	147.304	0	0.028	0.0363	5.1539	0.018	0.0775	0.312
NiO/Ni	0.967	90.598	8.85	5.578	2.7071	13.7444	0.019	5.5772	3.979
Ni _{0.99} Zn _{0.01} O/Ni	1.578	101.630	10.82	8.263	4.0286	13.6811	0.014	8.1930	4.688
Ni _{0.97} Zn _{0.03} O/Ni	1.034	86.694	9.93	6.920	3.2729	14.1016	0.011	6.8046	3.122
Ni _{0.95} Zn _{0.05} O/Ni	0.586	179.867	3.60	2.154	1.0393	13.8210	0.015	2.1767	2.546
Ni _{0.93} Zn _{0.07} O/Ni	1.200	104.323	12.72	6.307	2.6958	15.6056	0.023	6.3143	3.927
Ni _{0.9} Zn _{0.1} O/Ni	1.016	101.624	12.69	5.313	2.3598	15.0174	0.019	5.2646	2.867

The first term in Eq. (7a) represents the contribution of the BMP's, second term is the matrix contribution. Here $M_0 = Nm_s$, N is the number of BMPs involved, m_s is the effective spontaneous moment per BMP, χ_m is the susceptibility of the matrix. The Langevin function, $L(x)$ is given by [84]

$$L(x) = \coth(x) - \frac{1}{x} \tag{7b}$$

$$\text{with } x = \frac{m_{\text{eff}}H}{K_B T} \tag{7c}$$

Now Eq. (7a) becomes

$$M = M_0 \left(\coth(x) - \frac{1}{x} \right) + \chi_m H \tag{8}$$

Figure 10 shows the experimental M-H data of NiO and $\text{Ni}_{1-x}\text{Zn}_x\text{O}/\text{Ni}$ ($x=0$ to 0.1) nanocomposite taken in first interval (i.e., 0 to H) measured at 300 K. The solid line corresponds to the fitted data to the experimental data as per Eq. (8). It is worth mentioning here that the $m_s = m_{\text{eff}}$ at high temperature. The values of M_0 , m_{eff} and χ_m obtained from the fitting of Eq. (8) to experimental data are listed in Table 4.

As shown in Table 4, the value of M_0 of NiO is very small as compared to $\text{Ni}_{1-x}\text{Zn}_x\text{O}/\text{Ni}$ nanocomposites whereas the variation of matrix susceptibility, χ_m is not remarkable in NiO and $\text{Ni}_{1-x}\text{Zn}_x\text{O}/\text{Ni}$ nanocomposites. It is also evident that the m_{eff} is of the order of 10^{-17} emu. The variation of m_{eff} with increasing Zn doping concentration is in accordance with the magnetization behavior as discussed above. This indicated that Zn doping influences the magnetic property of

NiO/Ni nanocomposites. The volume concentration of BMP calculated from M_0 and m_{eff} is in the order of 10^{17} cm^{-3} . The required concentration of BMPs in order to have long-range percolation and to explain ferromagnetism is of the order of 10^{20} cm^{-3} [85, 86]. Therefore, this model alone cannot explain the occurrence of ferromagnetism to our case. Similar observation has also been reported for Co-doped ZnO samples [87].

The value of saturation magnetization of the samples can be obtained by fitting the high field (> 1 Tesla) magnetic hysteresis to following equation [88, 89]:

$$M = M_s \left(1 - \frac{8}{105} \left(\frac{K_1}{M_s H} \right)^2 \right) + kH \tag{9}$$

where M_s is the saturation magnetization, K_1 is the cubic anisotropic constant and k is the high field susceptibility. Figure 11 shows the room temperature M-H data taken in first interval (i.e., 0 to H) for NiO and $\text{Ni}_{1-x}\text{Zn}_x\text{O}/\text{Ni}$ ($x=0$ to 0.1) nanocomposite fitted to Eq. (9) beyond 20,000 Oe. The values of M_s and K_1 obtained from the fitting are reflected in Table 4. Magnetocrystalline anisotropy constant is one of the important characteristic features of the ferromagnetic substance. Generally, hard magnetic materials show larger magnetocrystalline anisotropy constant which enables to use them for application in magnetic recording media [90]. Franco and Silva [88] reported the value of magnetocrystalline anisotropy constant as $3.87 \times 10^6 \text{ erg/cm}^3$ for CoFe_2O_4 . Kumar and Kar [90] reported that the magnetocrystalline anisotropy constant of $\text{CoFe}_{2-x}\text{Al}_x\text{O}_4$ varies from $4.3 \times 10^4 \text{ erg/cm}^3$ to $0.4 \times 10^4 \text{ erg/cm}^3$ with changing the Al concentration x from 0 to 0.04. Kumar et al. [91] reported that the magnetocrystalline anisotropy

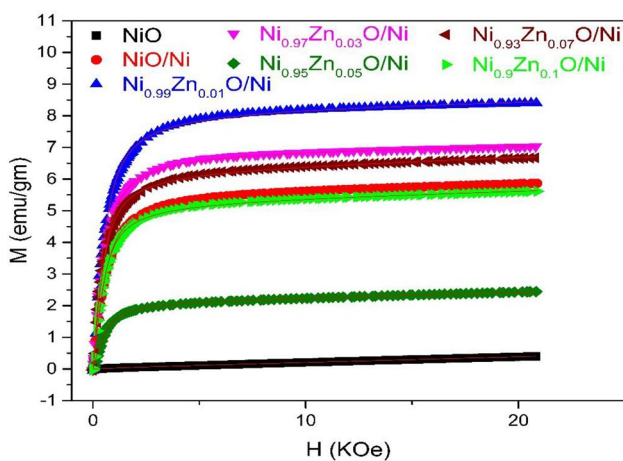


Fig. 10 Variation of magnetization with magnetic field for NiO and $\text{Ni}_{1-x}\text{Zn}_x\text{O}/\text{Ni}$ ($x=0$ to 0.1) nanocomposite taken in first interval (i.e., 0 to H) measured at 300 K. The solid line corresponds to the fitted data to the experimental data as per Eq. (8)

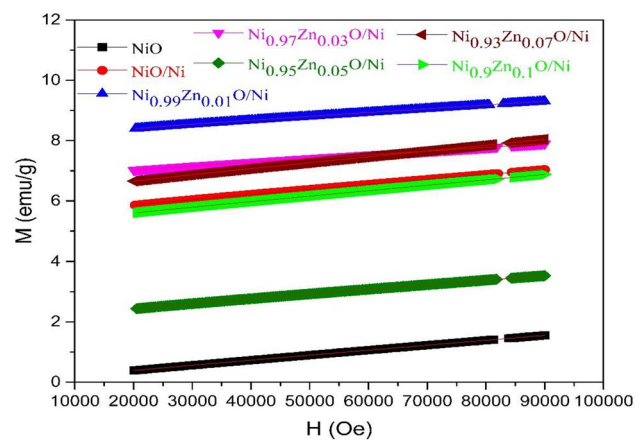


Fig. 11 Variation of magnetization with magnetic field for NiO and $\text{Ni}_{1-x}\text{Zn}_x\text{O}/\text{Ni}$ ($x=0$ to 0.1) nanocomposite taken in first interval (i.e., 0 to H) measured at 300 K. The solid line corresponds to the fitted data to the experimental data beyond 20,000 Oe as per Eq. (9)

constant of CoFe_2O_4 decreased from 4.522×10^5 erg/g to 2.421×10^5 erg/g while making nanocomposite with NiO in ratio of 0.5:0.5. In our case, the magnetocrystalline anisotropy constant of $\text{Ni}_{1-x}\text{Zn}_x\text{O}/\text{Ni}$ varies from 3.979×10^4 erg/g to 2.867×10^4 erg/g as Zn concentration changes from $x=0$ to 0.1 (Table 4).

The magnetization of the ferromagnetic materials can be fitted to Brillouin function and can be expressed [69] as

$$M_{\text{Brillouin}} = N'gJ\mu_B \left[\frac{2J+1}{2J} \coth \left(\frac{(2J+1)x}{2J} \right) - \frac{1}{2J} \coth \left(\frac{x}{2J} \right) \right] \tag{10}$$

where $x = \frac{gJ\mu_B H}{k_B T}$, J is the total electronic angular momentum, g is the Lande g factor of the magnetic ion, μ_B is the Bohr magneton, N' is the number of cation sites per gram, k_B is the Boltzmann constant. Since all the samples in our case show ferromagnetic behavior, we therefore fit magnetization data of first interval (i.e., 0 to H) measured at 300 K to Eq. (10). However, our magnetization data are not well fitted Eq. (10).

It has been reported that the magnetization of system with the distribution of magnetic ions as meagerly dispersed in large clusters can be well explained to following expression [92, 93]:

$$M_{\text{Brillouin-(H-A)model}} = M_{\text{Brillouin}} + M_{(H-A)\text{model}} \tag{11}$$

$$M_{(H-A)\text{model}} = \frac{AH}{(B+H)} \tag{12}$$

where A and B are the parameters in the H-A model. Also the H-A model explains the magnetization of the materials comprising of random defects as per Brown's theory [93]. Since our samples contain some type of defects, we therefore fit the magnetization data to Eq. (11). Since the Ni^{2+} ion has $S = 1$ and $L = 3$ with $J = 4$ [71, 94], we therefore fitted the magnetization curves (Fig. 12) of $\text{Ni}_{1-x}\text{Zn}_x\text{O}/\text{Ni}$ and NiO samples to $J = 4$ and our data nicely fitted to Eq. (11). The values of N' , A and B for NiO and $\text{Ni}_{1-x}\text{Zn}_x\text{O}/\text{Ni}$ obtained from fitting of the M-H curve with Eq. (11) are presented in Table 5.

4 Conclusion

We report the evolution of structural, optical and magnetic properties of $\text{Ni}_{1-x}\text{Zn}_x\text{O}/\text{Ni}$ ($x=0$ to 0.1) nanocomposite. Zn doping in NiO/Ni composite does not affect the crystal structure of NiO/Ni samples. However, the microstructure of composite sample is affected by Zn doping. The bond lengths among different ions increased with increasing Zn doping concentration. The redshift of OH stretching vibrations with increasing Zn

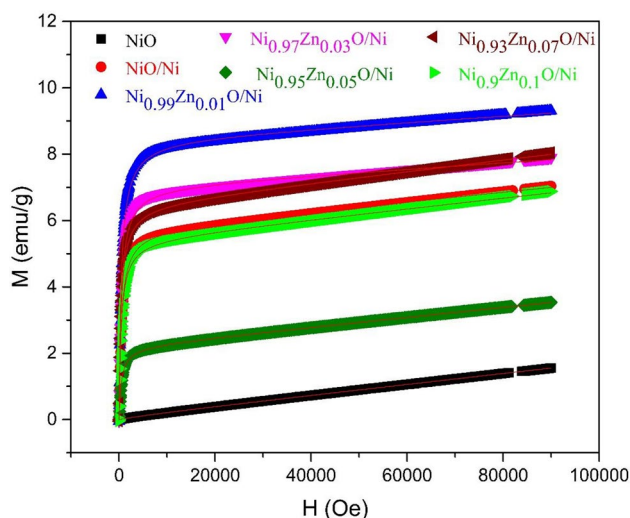


Fig. 12 Variation of magnetization with magnetic field for NiO and $\text{Ni}_{1-x}\text{Zn}_x\text{O}/\text{Ni}$ ($x=0$ to 0.1) nanocomposite taken in first interval (i.e., 0 to H) measured at 300 K. The solid line corresponds to the fitted data to the experimental data as per Eq. (11)

Table 5 The values of N' , A and B for NiO and $\text{Ni}_{1-x}\text{Zn}_x\text{O}/\text{Ni}$ obtained from fitting of the M-H curve with Eq. (11)

Sample	N' ($\times 10^{20}$) (per gm)	A (emu/gm)	B (Oe)
NiO	2.967	0.0854	9289.248
NiO/Ni	2.612	5.7314	495.361
$\text{Ni}_{0.99}\text{Zn}_{0.01}\text{O}/\text{Ni}$	1.645	8.4658	499.193
$\text{Ni}_{0.97}\text{Zn}_{0.03}\text{O}/\text{Ni}$	1.665	7.0400	470.648
$\text{Ni}_{0.95}\text{Zn}_{0.05}\text{O}/\text{Ni}$	2.696	2.2004	493.566
$\text{Ni}_{0.93}\text{Zn}_{0.07}\text{O}/\text{Ni}$	3.093	6.4878	439.584
$\text{Ni}_{0.9}\text{Zn}_{0.1}\text{O}/\text{Ni}$	2.879	5.4294	449.731

concentration in NiO could due to effect of Zn doping-induced modification in chemical environment. The band gap of NiO increased with increasing of Zn concentration. The occurrence of negative bowing in band gap is an indication that the nanocomposite could be useful for UV photodetector applications. Magnetic characterization on the samples indicated that NiO and all the $\text{Ni}_{1-x}\text{Zn}_x\text{O}/\text{Ni}$ samples show room temperature ferromagnetism. However, the nanocomposite sample with 1% Zn with the highest value remanent magnetization and anisotropic constant could be ideal for its use in various device applications like magnetic recording media.

Acknowledgements We thank Dr. P.V. Rajesh, UGC-DAE CSR, Kolkata Centre for his help in XRD measurements and H.O.D., Dept. of

Chemistry, NOU for providing FTIR and UV-Visible spectrometer facilities. PM and UKP thank UGC-DAE CSR, Mumbai Centre for providing financial support vide the Collaborative Research Project (CRS-M-241).

Compliance with ethical standards

Conflict of interest We do not have any conflict of interest at this moment.

References

- Roy R, Roy RA, Roy DM (1986) Alternative perspectives on “quasi-crystallinity”: non-uniformity and nanocomposites. *Mater Lett* 4:323–328. [https://doi.org/10.1016/0167-577X\(86\)90063-7](https://doi.org/10.1016/0167-577X(86)90063-7)
- Kremenović A, Jančar B, Ristić M et al (2012) Exchange-bias and grain-surface relaxations in nanostructured NiO/Ni induced by a particle size reduction. *J Phys Chem C* 116:4356–4364. <https://doi.org/10.1021/jp206658v>
- Camargo PHC, Satyanarayana KG, Wypych F (2009) Nanocomposites: synthesis, structure, properties and new application opportunities. *Mater Res* 12:1–39. <https://doi.org/10.1590/S1516-14392009000100002>
- Zeng H, Sun S (2008) Syntheses, properties, and potential applications of multicomponent magnetic nanoparticles. *Adv Funct Mater* 18:391–400. <https://doi.org/10.1002/adfm.200701211>
- Sun M, Liu H, Liu Y et al (2015) Graphene-based transition metal oxide nanocomposites for the oxygen reduction reaction. *Nanoscale* 7:1250–1269. <https://doi.org/10.1039/C4NR05838K>
- Radovic M, Lara-Curzio E (2004) Elastic properties of nickel-based anodes for solid oxide fuel cells as a function of the fraction of reduced NiO. *J Am Ceram Soc* 87:2242–2246. <https://doi.org/10.1111/j.1151-2916.2004.tb07499.x>
- Fan L, Zhu B, Chen M et al (2012) High performance transition metal oxide composite cathode for low temperature solid oxide fuel cells. *J Power Sources* 203:65–71. <https://doi.org/10.1016/j.jpowsour.2011.12.017>
- Skumryev V, Stoyanov S, Zhang Y et al (2003) Beating the superparamagnetic limit with exchange bias. *Nature* 423:850–853. <https://doi.org/10.1038/nature01687>
- Nelson PA, Owen JR (2003) A high-performance supercapacitor/battery hybrid incorporating templated mesoporous electrodes. *J Electrochem Soc* 150:A1313. <https://doi.org/10.1149/1.1603247>
- Wen W, Wu J-M (2011) Eruption combustion synthesis of NiO/Ni nanocomposites with enhanced properties for dye-absorption and lithium storage. *ACS Appl Mater Interfaces* 3:4112–4119. <https://doi.org/10.1021/am2010064>
- Zou F, Chen Y-M, Liu K et al (2016) Metal organic frameworks derived hierarchical hollow NiO/Ni/graphene composites for lithium and sodium storage. *ACS Nano* 10:377–386. <https://doi.org/10.1021/acsnano.5b05041>
- Das HT, Mahendraprabhu K, Maiyalagan T, Elumalai P (2017) Performance of solid-state hybrid energy-storage device using reduced graphene-oxide anchored sol-gel derived Ni/NiO nanocomposite. *Sci Rep* 7:15342
- Adhikari S, Madras G (2017) Role of Ni in hetero-architected NiO/Ni composites for enhanced catalytic performance. *Phys Chem Chem Phys* 19:13895–13908. <https://doi.org/10.1039/C7CP01332A>
- Harras FA, Mohamed RM, Shawky A, Ibrahim IA (2010) Composition and phase control of Ni/NiO nanoparticles for photocatalytic degradation of EDTA. *J Alloys Compd* 508:133–140. <https://doi.org/10.1016/j.jallcom.2010.08.027>
- You W, Che R (2018) Excellent NiO–Ni nanoplate microwave absorber via pinning effect of antiferromagnetic-ferromagnetic interface. *ACS Appl Mater Interfaces* 10:15104–15111. <https://doi.org/10.1021/acsami.8b03610>
- Ganeshchandra Prabhu V, Shajira PS, Lakshmi N, Junaid Bushiri M (2015) Magnetic properties of Ni/NiO nanocomposites synthesized by one step solution combustion method. *J Phys Chem Solids* 87:238–243. <https://doi.org/10.1016/j.jpcs.2015.09.001>
- Lee IS, Lee N, Park J et al (2006) Ni/NiO Core/shell nanoparticles for selective binding and magnetic separation of histidine-tagged proteins. *J Am Chem Soc* 128:10658–10659. <https://doi.org/10.1021/ja063177n>
- Thota S, Shim JH, Seehra MS (2013) Size-dependent shifts of the Néel temperature and optical band-gap in NiO nanoparticles. *J Appl Phys* 114:214307. <https://doi.org/10.1063/1.4838915>
- Bahl CRH, Hansen MF, Pedersen T et al (2006) The magnetic moment of NiO nanoparticles determined by Mössbauer spectroscopy. *J Phys: Condens Matter* 18:4161–4175. <https://doi.org/10.1088/0953-8984/18/17/005>
- Rinaldi-Montes N, Gorria P, Martínez-Blanco D et al (2015) Scrutinizing the role of size reduction on the exchange bias and dynamic magnetic behavior in NiO nanoparticles. *Nanotechnology* 26:305705. <https://doi.org/10.1088/0957-4484/26/30/305705>
- Rostamnejadi A, Bagheri S (2017) Optical, magnetic, and microwave properties of Ni/NiO nanoparticles. *Appl Phys A* 123:233. <https://doi.org/10.1007/s00339-017-0853-1>
- Master R, Karandikar M, Jambhale A et al (2014) Zn doping induced ferromagnetism in NiO. *J Phys: Conf Ser* 534:012025. <https://doi.org/10.1088/1742-6596/534/1/012025>
- Sathishkumar K, Shanmugam N, Kannadasan N et al (2014) Influence of Zn²⁺ ions incorporation on the magnetic and pseudo capacitance behaviors of NiO nanoparticles. *Mater Sci Semicond Process* 27:846–853. <https://doi.org/10.1016/j.mssp.2014.08.025>
- Bharathy G, Raji P (2015) Synthesis and magnetic properties of pure and Zn doped NiO nanoparticles. *Int J ChemTech Res* 7:1559–1562
- Huang XH, Tu JP, Zhang B et al (2006) Electrochemical properties of NiO–Ni nanocomposite as anode material for lithium ion batteries. *J Power Sources* 161:541–544. <https://doi.org/10.1016/j.jpowsour.2006.03.039>
- Lai H, Wu Q, Zhao J et al (2016) Mesostructured NiO/Ni composites for high-performance electrochemical energy storage. *Energy Environ Sci* 9:2053–2060. <https://doi.org/10.1039/C6EE00603E>
- Silva RM, Raimundo RA, Fernandes WV et al (2018) Proteic sol-gel synthesis, structure and magnetic properties of Ni/NiO core-shell powders. *Ceram Int* 44:6152–6156. <https://doi.org/10.1016/j.ceramint.2017.12.248>
- Cui WB, Hu WJ, Zhang YJ et al (2009) Cooling-field dependence of exchange bias in Mg-diluted Ni_{1-x}Mg_xO/Ni granular systems. *J Magn Magn Mater* 321:1943–1946. <https://doi.org/10.1016/j.jmmm.2008.12.016>
- Joughehdoust S, Manafi S, Aslan MH et al (2011) Determination of microstructural parameters of nanocrystalline hydroxyapatite prepared by mechanical alloying method. *AIP Conf Proc* 1400:486–491
- Rodríguez-Carvajal J (1993) Recent advances in magnetic structure determination by neutron powder diffraction. *Phys B Condens Matter* 192:55–69. [https://doi.org/10.1016/0921-4526\(93\)90108-l](https://doi.org/10.1016/0921-4526(93)90108-l)
- Singh SD, Nandanwar V, Srivastava H et al (2015) Determination of the optical gap bowing parameter for ternary Ni_{1-x}Zn_x

- O cubic rocksalt solid solutions. *Dalton Trans* 44:14793–14798. <https://doi.org/10.1039/C5DT02283E>
32. Singh SD, Poswal AK, Kamal C et al (2017) Bond length variation in Zn substituted NiO studied from extended X-ray absorption fine structure. *Solid State Commun* 259:40–44. <https://doi.org/10.1016/j.ssc.2017.05.002>
 33. Nowsath Rifaya M, Theivasanthi T, Alagar M (2012) Chemical capping synthesis of nickel oxide nanoparticles and their characterizations studies. *Nanosci Nanotechnol* 2:134–138. <https://doi.org/10.5923/j.nn.20120205.01>
 34. Thangamani C, Pushpanathan K (2016) Optical and dielectric behavior of NiO: Zn quantum dots. *J Chem Pharm Res* 8:749–757
 35. Dang LX, Pettitt BM (1987) Simple intramolecular model potentials for water. *J Phys Chem* 91:3349–3354. <https://doi.org/10.1021/j100296a048>
 36. Coker DF, Miller RE, Watts RO (1985) The infrared predissociation spectra of water clusters. *J Chem Phys* 82:3554–3562. <https://doi.org/10.1063/1.448935>
 37. Reimers JR, Watts RO (1984) The structure, thermodynamic properties and infrared spectra of liquid water and ice. *Chem Phys* 91:201–223. [https://doi.org/10.1016/0301-0104\(84\)80055-5](https://doi.org/10.1016/0301-0104(84)80055-5)
 38. Toukan K, Rahman A (1985) Molecular-dynamics study of atomic motions in water. *Phys Rev B* 31:2643–2648. <https://doi.org/10.1103/PhysRevB.31.2643>
 39. Bopp P, Jancsó G, Heinzinger K (1983) An improved potential for non-rigid water molecules in the liquid phase. *Chem Phys Lett* 98:129–133. [https://doi.org/10.1016/0009-2614\(83\)87112-7](https://doi.org/10.1016/0009-2614(83)87112-7)
 40. Kalam A, Al-Sehemi AG, Al-Shihri AS et al (2012) Synthesis and characterization of NiO nanoparticles by thermal decomposition of nickel linoleate and their optical properties. *Mater Charact* 68:77–81. <https://doi.org/10.1016/j.matchar.2012.03.011>
 41. Dewan S, Tomar M, Tandon RP, Gupta V (2017) Zn doping induced conductivity transformation in NiO films for realization of p-n homo junction diode. *J Appl Phys* 121:215307. <https://doi.org/10.1063/1.4984580>
 42. Agrawal S, Parveen A, Azam A (2017) Microwave assisted synthesis of Co doped NiO nanoparticles and its fluorescence properties. *J Lumin* 184:250–255. <https://doi.org/10.1016/j.jlumi.2016.12.035>
 43. Banerjee D, Ghosh CK, Duari B et al (2014) Failure analysis of resin of different coating materials by infrared spectroscopy. *Int J Latest Res Sci Technol* 3:105–108
 44. Xin X, Lü Z, Zhou B et al (2007) Effect of synthesis conditions on the performance of weakly agglomerated nanocrystalline NiO. *J Alloys Compd* 427:251–255. <https://doi.org/10.1016/j.jallcom.2006.02.064>
 45. Coates J (2006) Interpretation of infrared spectra, a practical approach. In: Meyers RA (ed) *Encyclopedia of analytical chemistry*. Wiley, Chichester
 46. Solaichamy R, Karpagam J (2016) Structural and Vibrational Studies (FT-IR, FT-Raman) of Voglibose Using DFT Calculation. *Int Lett Chem Phys Astron* 64:45–62. <https://doi.org/10.18052/www.scipress.com/ILCPA.64.45>
 47. Bharathy G, Raji P (2017) Room temperature ferromagnetic behavior of Mn doped NiO nanoparticles: a suitable electrode material for supercapacitors. *J Mater Sci: Mater Electron* 28:17889–17895. <https://doi.org/10.1007/s10854-017-7730-8>
 48. Kunasekaran V, Krishnamoorthy K (2015) Compatibility studies of rasagiline mesylate with selected excipients for an effective solid lipid nanoparticles formulation. *Int J Pharm Pharm Sci* 7:73–80
 49. Zahariev I, Piskin M, Karaduman E et al (2017) FTIR spectroscopy method for investigation of Co-Ni nanoparticle nanosurface phenomena. *J Chem Technol Metall* 52:916–928
 50. Thangamani C, Pushpanathan K (2018) Synthesis and characterization of NiZnO nanoparticles. *Inorg Nano-Met Chem* 48:131–138. <https://doi.org/10.1080/24701556.2017.1373294>
 51. Mott NF, Davis EA (2012) *Electronic processes in non-crystalline materials*. Oxford University Press, Oxford
 52. Mallick P, Rath C, Prakash J et al (2010) Swift heavy ion irradiation induced modification of the microstructure of NiO thin films. *Nucl Instrum Methods Phys Res Sect B Beam Interact Mater At* 268:1613–1617. <https://doi.org/10.1016/j.nimb.2010.02.005>
 53. Mohammadjoo M, Khorshidi ZN, Sadrnezhad SK, Mazinani V (2014) Original article synthesis and characterization of nickel oxide nanoparticle with wide band gap energy prepared via thermochemical processing. *Nanosci Nanotechnol Int J* 4:6–9
 54. Sharma R, Acharya AD, Shrivastava SB et al (2016) Studies on the structure optical and electrical properties of Zn-doped NiO thin films grown by spray pyrolysis. *Opt Int J Light Electron Opt* 127:4661–4668. <https://doi.org/10.1016/j.ijleo.2016.01.050>
 55. Hashim FS, Sami NA (2015) Effect of Zn doping on structural and some optical studies of nano NiO films prepared by Sol-Gel technique. *Int Lett Chem Phys Astron* 53:31–40. <https://doi.org/10.18052/www.scipress.com/ILCPA.53.31>
 56. Manouchehri I, AlShiaa SAO, Mehrparparvar D et al (2016) Optical properties of zinc doped NiO thin films deposited by RF magnetron sputtering. *Optik* 127:9400–9406. <https://doi.org/10.1016/j.ijleo.2016.06.092>
 57. Dixit H, Saniz R, Lamoen D, Partoens B (2010) The quasiparticle band structure of zincblende and rocksalt ZnO. *J Phys: Condens Matter* 22:125505. <https://doi.org/10.1088/0953-8984/22/12/125505>
 58. Bernard JE, Zunger A (1986) Optical bowing in zinc chalcogenide semiconductor alloys. *Phys Rev B* 34:5992–5995. <https://doi.org/10.1103/PhysRevB.34.5992>
 59. Mallick P (2018) Evolution of optical band gap and related properties in Ni_{1-x}Co_xO Nanoparticles. *Natl Acad Sci Lett*. <https://doi.org/10.1007/s40009-018-0727-x>
 60. Kumar V, Singh JK (2010) Model for calculating the refractive index of different materials. *Indian J Pure Appl Phys* 48:571–574
 61. Ahmad S, Ashraf M, Ahmad A, Singh DV (2013) Electronic and optical properties of semiconductor and alkali halides. *Arab J Sci Eng* 38:1889–1894. <https://doi.org/10.1007/s13369-013-0551-z>
 62. Mallick P, Mishra DK, Kumar P, Kanjilal D (2015) UV-Vis studies of 800 keV Ar ion irradiated NiO thin films. *Mater Sci Pol* 33:555–559. <https://doi.org/10.1515/msp-2015-0082>
 63. Mallick P (2017) Effect of solvent on the microstructure and optical band gap of ZnO nanoparticles. *Indian J Pure Appl Phys* 55:187–192
 64. Winkler E, Zysler RD, Vasquez Mansilla M et al (2008) Surface spin-glass freezing in interacting core-shell NiO nanoparticles. *Nanotechnology* 19:185702. <https://doi.org/10.1088/0957-4484/19/18/185702>
 65. Meneses CT, Duque JGS, de Biasi E et al (2010) Competing interparticle interactions and surface anisotropy in NiO nanoparticles. *J Appl Phys* 108:013909. <https://doi.org/10.1063/1.3459890>
 66. Tadić M, Panjan M, Marković D et al (2011) Unusual magnetic properties of NiO nanoparticles embedded in a silica matrix. *J Alloys Compd* 509:7134–7138. <https://doi.org/10.1016/j.jallcom.2011.04.032>
 67. Shahzad F, Nadeem K, Weber J et al (2017) Magnetic behavior of NiO nanoparticles determined by SQUID magnetometry. *Mater Res Express* 4:086102. <https://doi.org/10.1088/2053-1591/aa8674>
 68. Winkler E, Zysler RD, Mansilla MV, Fiorani D (2005) Surface anisotropy effects in NiO nanoparticles. *Phys Rev B* 72:132409. <https://doi.org/10.1103/PhysRevB.72.132409>

69. Kittel C (2005) Introduction to solid state physics, 8th edn. Wiley, Hoboken
70. Correa EL, Bosch-Santos B, Cavalcante FHM et al (2016) Properties of Gd_2O_3 nanoparticles studied by hyperfine interactions and magnetization measurements. *AIP Adv* 6:056112. <https://doi.org/10.1063/1.4943601>
71. Cotton FA, Wilkinson G (1980) Advanced inorganic chemistry, 4th edn. Wiley
72. Peck MA, Huh Y, Skomski R et al (2011) Magnetic properties of NiO and (Ni, Zn)O nanoclusters. *J Appl Phys* 109:07B518. <https://doi.org/10.1063/1.3556953>
73. Narsinga Rao G, Yao YD, Chen JW (2009) Evolution of size, morphology, and magnetic properties of CuO nanoparticles by thermal annealing. *J Appl Phys* 105:093901. <https://doi.org/10.1063/1.3120785>
74. Madhu G, Maniammal K, Biju V (2016) Defect induced ferromagnetic interaction in nanostructured nickel oxide with core-shell magnetic structure: the role of Ni^{2+} and O^{2-} vacancies. *Phys Chem Chem Phys* 18:12135–12148. <https://doi.org/10.1039/C5CP03710G>
75. Li L, Chen L, Qihe R, Li G (2006) Magnetic crossover of NiO nanocrystals at room temperature. *Appl Phys Lett* 89:134102. <https://doi.org/10.1063/1.2357562>
76. Mallick P, Rath C, Rath A et al (2010) Antiferro to superparamagnetic transition on Mn doping in NiO. *Solid State Commun* 150:1342–1345. <https://doi.org/10.1016/j.ssc.2010.05.003>
77. Du F, Bie X, Bian X et al (2013) Preparation, structure and magnetic properties of lithium substituted NiO by molten salt method. *Chem Res Chin Univ* 29:210–213. <https://doi.org/10.1007/s40242-013-2159-y>
78. Hsu HS, Huang JCA, Huang YH et al (2006) Evidence of oxygen vacancy enhanced room-temperature ferromagnetism in Co-doped ZnO. *Appl Phys Lett* 88:242507. <https://doi.org/10.1063/1.2212277>
79. Pal B, Giri PK (2010) High temperature ferromagnetism and optical properties of Co doped ZnO nanoparticles. *J Appl Phys* 108:084322. <https://doi.org/10.1063/1.3500380>
80. McCabe GH, Fries T, Liu MT et al (1997) Bound magnetic polarons in p-type $Cu_2Mn_{0.9}Zn_{0.1}SnS_4$. *Phys Rev B* 56:6673–6680. <https://doi.org/10.1103/PhysRevB.56.6673>
81. Zunger A, Lany S, Raebiger H (2010) The quest for dilute ferromagnetism in semiconductors: guides and misguides by theory. *Physics* 3:53. <https://doi.org/10.1103/Physics.3.53>
82. Chiorescu C, Cohn JL, Neumeier JJ (2007) Impurity conduction and magnetic polarons in antiferromagnetic oxides. *Phys Rev B* 76:020404. <https://doi.org/10.1103/PhysRevB.76.020404>
83. Dietl T, Spalek J, Świerkowski L (1986) Theory of the bound magnetic polaron: a physical discussion and a comment. *Phys Rev B* 33:7303–7306. <https://doi.org/10.1103/PhysRevB.33.7303>
84. Bora T, Samantaray B, Mohanty S, Ravi S (2011) Ferromagnetism and bound magnetic polaron behavior in $(In_{1-x}Co_x)_2O_3$. *IEEE Trans Magn* 47:3991–3994. <https://doi.org/10.1109/TMAG.2011.2157660>
85. Coey JMD, Venkatesan M, Fitzgerald CB (2005) Donor impurity band exchange in dilute ferromagnetic oxides. *Nat Mater* 4:173–179. <https://doi.org/10.1038/nmat1310>
86. Pal B, Sarkar D, Giri PK (2015) Structural, optical, and magnetic properties of Ni doped ZnO nanoparticles: correlation of magnetic moment with defect density. *Appl Surf Sci* 356:804–811. <https://doi.org/10.1016/j.apsusc.2015.08.163>
87. Srinet G, Varshney P, Kumar R et al (2013) Structural, optical and magnetic properties of $Zn_{1-x}Co_xO$ prepared by the sol-gel route. *Ceram Int* 39:6077–6085. <https://doi.org/10.1016/j.ceramint.2013.01.025>
88. Franco A, e Silva FC (2010) High temperature magnetic properties of cobalt ferrite nanoparticles. *Appl Phys Lett* 96:172505. <https://doi.org/10.1063/1.3422478>
89. Chikazumi S, Graham CD, Chikazumi S (1997) Physics of ferromagnetism, 2nd edn. Oxford University Press, Oxford
90. Kumar L, Kar M (2011) Influence of Al^{3+} ion concentration on the crystal structure and magnetic anisotropy of nanocrystalline spinel cobalt ferrite. *J Magn Magn Mater* 323:2042–2048. <https://doi.org/10.1016/j.jmmm.2011.03.010>
91. Kumar R, Singh RK, Kar M (2018) Magnetic interaction between ferrimagnetic $CoFe_2O_4$ and antiferromagnetic NiO in nanocomposite. *Phys B Phys Condens Matter* 530:114–120. <https://doi.org/10.1016/j.physb.2017.11.017>
92. Valente MA, Mendiratta SK (1999) High Field magnetization of glasses. *J Non-Cryst Solids* 247:26–30
93. Alborzi Avnaki Z, Hassanzadeh A (2013) Modified Brillouin function to explain the ferromagnetic behavior of surfactant-aided synthesized $\alpha-Fe_2O_3$ nanostructures. *J Theor Appl Phys* 7:19. <https://doi.org/10.1186/2251-7235-7-19>
94. Coey JMD, Venkatesan M, Xu H (2013) Introduction to magnetic oxides. In: Ogale SB, Venkatesan TV, Blamire MG (eds) Functional metal oxides. Wiley-VCH Verlag GmbH & Co. KGaA, Weinheim, pp 1–49

Publisher's Note Springer Nature remains neutral with regard to jurisdictional claims in published maps and institutional affiliations.